Available online at BCREC website: https://journal.bcrec.id/index.php/bcrec

Bulletin of Chemical Reaction Engineering & Catalysis, 19 (1) 2024, 32-46

Research Article

NO Dissociation on Platinum and Platinum-Rhodium Alloy: A Theoretical Investigation

Khanh B. Vu[1,2]*, Khoa Thanh Phung[1,2], Le Hoang Thong[1,2], Bui Thi Linh[1,2], Nguyen Ngoc Huyen[1,2]

[1]Department of Chemical and Environmental Engineering, International University, Ho Chi Minh City, Vietnam
[2]Vietnam National University, Ho Chi Minh City, Vietnam.

Received: 7th November 2023; Revised: 22nd December 2023; Accepted: 23rd December 2023
Available online: 26th December 2023; Published regularly: April 2024

Abstract

In this computational study, the preferential adsorption and co-adsorption sites of various chemical species (N, O, and NO) on the Pt (111) and Rh_3Pt (111) surfaces were identified. The preferential adsorption site for NO and co-adsorption sites for N and O on the Pt (111) surface are the hollow (fcc) sites; and these on the Rh_3Pt (111) surface are the hollow (fcc1) site and hollow N(hcp2)-O(fcc1) sites, respectively. The activation energies of the NO dissociation reaction on the Pt (111) and Rh_3Pt (111) catalytic surfaces are 2.35 and 2.02 eV, respectively. The lower activation energy of the NO decomposition on the Rh_3Pt (111) surface is explained by the stronger back-donation from the 4d orbital of the Rh atoms to the $2\pi^*$ anti-bonding orbital of the NO molecule. The activation energies of the N and O recombination reaction on the Pt (111) and Rh_3Pt (111) catalytic surfaces are 1.51 and 2.30 eV, respectively. The study indicates that the Rh_3Pt (111) surface not only facilitates the NO decomposition but also better prevents N and O from recombination.

Keywords: NO dissociation; Quantum ESPRESSO; Platinum; Rhodium; Catalysis

How to Cite: Vu, K.B., Phung, K.T., Thong, L.H., Linh, B.T., Huyen, N.N. (2024). NO Dissociation on Platinum and Platinum-Rhodium Alloy: A Theoretical Investigation. *Bulletin of Chemical Reaction Engineering & Catalysis*, 19(1), 32-46 (doi: 10.9767/bcrec.20070)

Permalink/DOI: https://doi.org/10.9767/bcrec.20070

Supporting Information : *https://journal.bcrec.id/index.php/bcrec/article/downloadSuppFile/20070/5112*

1. Introduction

The emission of nitric oxide is unavoidable; therefore, the treatment for this pollutant is necessary. The selection of the treatment method depends on several factors such as the emission source, concentration, regulations, economic consideration, and available infrastructure. A combination of several methods can be applied to optimize the treatment process. Some typical treatment methods include: i) selective catalytic reduction [1]: this method uses catalysts to reduce the NO gas emitted from power plants, industrial processes, and vehicles. The NO gas reacts with a reducing agent like ammonia or urea over a catalyst to produce nitrogen and water. This method is highly efficient and selective and potentially applied for large-scale treatment, but catalysts are prone to poisoning due to contaminants in feedstock in addition to ammonia slip and reducing agent cost; ii) non-thermal plasma treatment [2,3]: passing a flow of NO gas through the reactor with high-voltage electrical discharge to form nitrogen oxides, which are further treated by other methods. This method offers a lower treatment temperature than traditional thermal methods; however, it costs much energy and potentially produces ozone as a byproduct; iii) absorption with basic solutions [4-6]: a stream of NO gas is passed

* Corresponding Author.
Email: vubkhanh@gmail.com (K. B. Vu)

through a basic solution such as alkaline- or amine-based solution. The absorbed NO gas is converted to nitrate or nitrite compounds for further treatment. This method is good for small scale and cost-effective due to simple equipment. However, we have to deal with solution handling and chemical waste generation; iv) catalytic decomposition [7,8]: conversion of NO gas to nitrogen and oxygen at high temperatures. It is efficient for NO removal and potentially utilized for high-temperature processes. The performance of catalysts is prone to contaminants in feedstock; v) other methods such as biological treatment [9,10], adsorption on the surface of porous materials [11-13], and combustion modification are also considered.

Among the above-mentioned methods, catalytic decomposition and selective catalytic reduction are popular for treatment of NO gas. Therefore, in this study, we focus on the catalytic decomposition of NO gas over heterogeneous catalysts. The catalytically active sites for this method include platinum [14,15], rhodium [16,17], palladium [18,19], copper [20], and iron [21]. Platinum and rhodium are highly active, stable at high-temperature working conditions, and effective for the removal of NO; its limitation includes high cost and sensitivity to poisoning [22]. Palladium exhibits effective at low temperature, but it is also an expensive material and poisoned by sulfur compounds [23]. Copper-based catalysts work at low temperatures and low cost but require oxygen as co-adsorption for acceptable activity. Copper is also prone to deactivation due to oxidation [24]. Ion-based catalysts are cheap and work at low temperatures. However, their activity is moderate compared to other catalysts, and they are also prone to deactivation. Due to their high activity and stability at high temperature, the noble metal catalysts including platinum, rhodium, and palladium have been commercialized, albeit their expensiveness. Finding noble catalysts with excellent activity for NO activation and working at low temperatures are still needed [25], and computational chemistry is an indispensable part of exploring process.

The reaction mechanism for catalytic decomposition of NO under lean conditions over platinum catalyst was generally accepted as follows [26]:

i) NO dissociation step: $NO^* \rightarrow N^* + O^*$;
ii) Nitrogen formation: $N^* + N^* \rightarrow N_2$;
iii) Byproduct formation: $NO^* + N^* \rightarrow N_2O$

Starred species indicate adsorption state on metallic surface, and non-starred species indicate gas phase.

NO is chemically dissociated on platinum surface and then produces gaseous nitrogen molecule. However, oxygen molecule is not formed because oxygen atoms strongly combine and poison platinum atoms. The formation of platinum oxide results in catalyst deactivation; therefore, NO dissociation is eventually eliminated. Therefore, reducing agent such as hydrogen or carbon monoxide is introduced to clean platinum surface, and NO dissociation reaction is still unaffected. The formation of N_2O is rather complicated because it can be considered as a main product or an intermediate, depending on studies [27-29]. The reaction mechanisms and energetic barriers of these reactions have been theoretically investigated on pure metallic surfaces such as platinum [30-33]. The commonly investigated surface of platinum catalyst is Pt (111) because of its energetic stability compared to other surfaces [34]. Recently, rhodium–cerium oxide clusters catalytically transforms NO to N_2 and CO_2 by reduction its reaction with CO. The intermediate N_2O is proposed to adsorb on the Rh atom in the cluster and dissociated to form N_2 molecule with the assistance of two Ce atoms [35]. Platinum-rhodium alloy catalysts have been used in many industrial applications as emission control, hydrogenation/dehydrogenation reactions [36], reduction of 4-nitrophenol and rhodamine B [37], photocatalytic degradation of methylene blue [38], hydrogen evolution [39], and nitric acid production.

As mentioned previously, the NO activation is the first and important step in the reaction mechanism for the catalytic decomposition of NO under lean conditions over platinum catalyst. We were curious how this activation step works on the platinum-rhodium alloy because the NO decomposition has not been theoretically investigated on the Rh_3Pt alloy. In this research, the adsorption of the N, O, and NO species and the activation energy of the NO decomposition on the Pt (111) and Rh_3Pt (111) surfaces were theoretically explored. In addition, the electronic interaction between the adsorbed NO molecule with the Pt (111) and Rh_3Pt (111) surfaces were studied through the projected density states of Pt 5d and Rh 4d.

2. Computational Method

The adsorption energies of the N, O, and NO species and activation energy of NO decomposition on catalyst surface were investigated using the Quantum ESPRESSO package [40,41]. The Pt (111) and Rh_3Pt (111) surfaces were created from the bulk Pt and Rh_3Pt struc-

tures, respectively. Both Pt (111) and Rh_3Pt (111) surfaces were selected for the calculations due to their energetic stability [34]. The calculations of Pt (111) and Rh_3Pt (111) systems were fully optimized by PWscf code using the Quantum ESPRESSO package. The interaction between core and valence electrons was described by the projector augmented wave (PAW) pseudopotential [42] or Vanderbilt ultrasoft pseudopotentials [43]. The valence electron configurations considered are: 2s 2p for O and N, 5d 6s 6p for Pt, and 4s 4p 4d 5p for Rh. The cut-off kinetic energy was set at 48 Ry. All atoms in lattice were fully relaxed until residue forces on constituent atoms were smaller than 1×10^{-8} eV/Å. The Monkhorst-Pack mesh of *k* points (5 x 5 x 1) was used for the atomic relaxation and electronic calculations. The spin-polarized was used in all calculations. The Pt (111) and Rh_3Pt (111) slab models are depicted in Figure 1. The slab consists of four layers of atoms; two bottom layers were fixed, and two top layers were allowed to relax during the atomic optimization.

3. Results and Discussion

3.1 Convergence tests for Pt (111) and Rh_3Pt (111) slabs

The kinetic energy cut-off (ecutwfc), charge density cut-off (ecutrho), Monkhorst-Pack mesh of *k* points, vacuum size, degauss values and smearing types have been investigated for both Pt (111) and Rh_3Pt (111) slabs to get the convergence parameters for further calculations. Figure 1S (Supporting Information) shows the convergence tests for the Pt (111) surface. The convergence parameters for Pt (111) are: ecutwfc >= 35 Ry, ecutrho >= 300 Ry, *k*-point >= 5 x 5 x 1, and vacuum gap >= 15 Å. The convergence tests for Rh_3Pt (111) are shown in Figure 2S (Supporting Information). The convergence parameters for Rh_3Pt (111) are: ecutwfc >= 40 Ry, ecutrho >= 300 Ry, *k*-point >= 5 x 5 x 1, and vacuum gap >= 15 Å. The final convergence parameters for both slabs have been selected to be as follows: ecutwfc = 48 Ry, ecutrho = 450 Ry, k-point = 5 x 5 x 1, and vacuum gap = 43 Å. The vacuum space has been extended to eliminate the interaction between adsorbates along z-axis.

The next convergence parameter have been tested are the type of smearing and degauss value for both slabs. The convergence test is shown in Figure 3S (Supporting Information) for different types of smearing: Marzari-Vanderbilt-DeVita-Payne cold smearing (mv), ordinary Gaussian spreading (Gaussian), Methfessel-Paxton first-order spreading (mp), and smearing with Fermi-Dirac function (fd). It shows that the suitable smearing type is cold smearing (mv) for both slabs with a wide applicable range of degauss values. Therefore, we selected the mv smearing for all calculations.

The dynamic stability of both Pt (111) and Rh_3Pt (111) slabs have been checked through the phonon calculations. The calculated results are presented in Figure 2. The phonon dispersions were computed using the ph.x program in Quantum ESPRESSO with implementation of density functional perturbation theory (DFPT). The phonon dispersion curves show that two slabs are dynamically stable because there are almost positive vibrations and small negative vibrations at gamma for both slabs.

3.2 Preferential Adsorption Sites and Activation Energy on Pt (111)

The preferential adsorption sites of molecules and atoms on the Pt (111) and Rh_3Pt (111) surfaces were calculated at the symmetrical positions on both slabs. The symmetrical

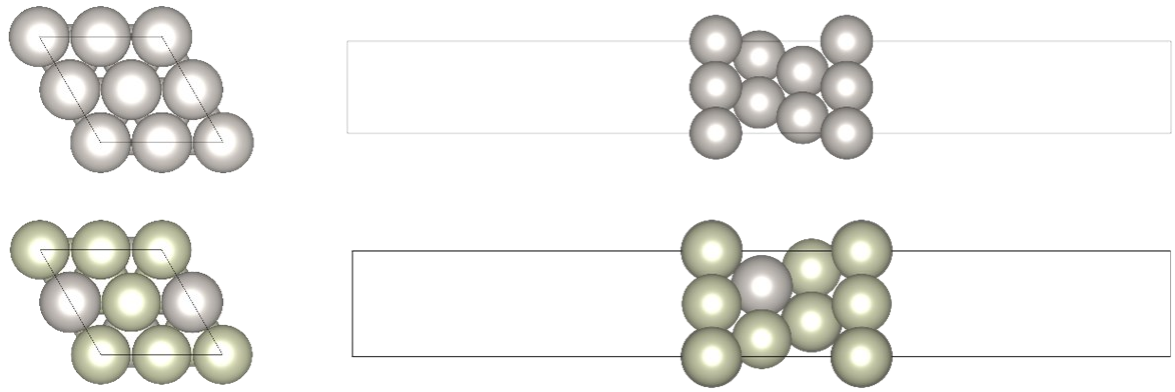

Figure 1. (2x2) unit cell of Pt (111) slab (top) and (2x2) unit cell of Rh_3Pt (111) slab (bottom). The gray and violet spheres represent Rh and Pt atoms, respectively. The vacuum gap along z-axis for both models is 43 Å. Each slab has four layers of atoms, and the number of atoms in each cell is 16.

sites on each slab are shown in Figure 3. The NO decomposition over the two surfaces was investigated, and the adsorption energies of the NO molecule, O and N atoms were evaluated through the following formula:

$E_{(ads)} = E_{(slab/NO)} - E_{(slab)} - E_{(NO)}$ for the NO molecule

$E_{(ads)} = E_{(slab/M)} - E_{(slab)} - 0.5*E_{(M)}$ for the O or N atom.

where, M is the O_2 or N_2 molecule. The adsorption energies of NO, O, and N over the Pt (111) surface are summarized in Table 1.

The preferential adsorption site on Pt (111) is fcc for three species – NO, N, and O. The preferential adsorption sites for NO, N, and O are consistent with the previous observation on the Pt (111) surface of a (2x2) unit cell [44]. The preferential adsorption sites for co-adsorption of N and O on the Pt (111) surface was also computed in terms of the adsorption energy. The calculated adsorption energies for co-adsorption of N and O on the symmetric sites of the P(111) surface are listed in Table 2.

The N and O atoms placed on different symmetrical sites are referred to the initial configurations. After performing calculations, the positions of N and O were changed and moved to more energetically stable sites, and these sites are referred to as the final configurations. The binding energies were evaluated using two types of pseudopotentials – PAW (projector-augmented wave) and ultrasoft GBRV for the

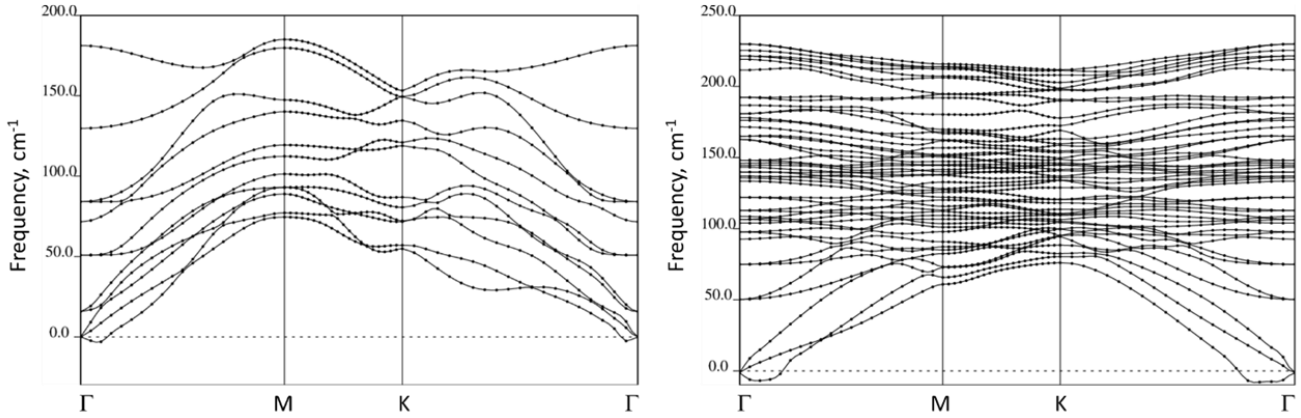

Figure 2. Phonon dispersion curves of (1x1) unit cell of Pt (111) (left) and (2x2) unit cell of Rh_3Pt (111) (right) slabs.

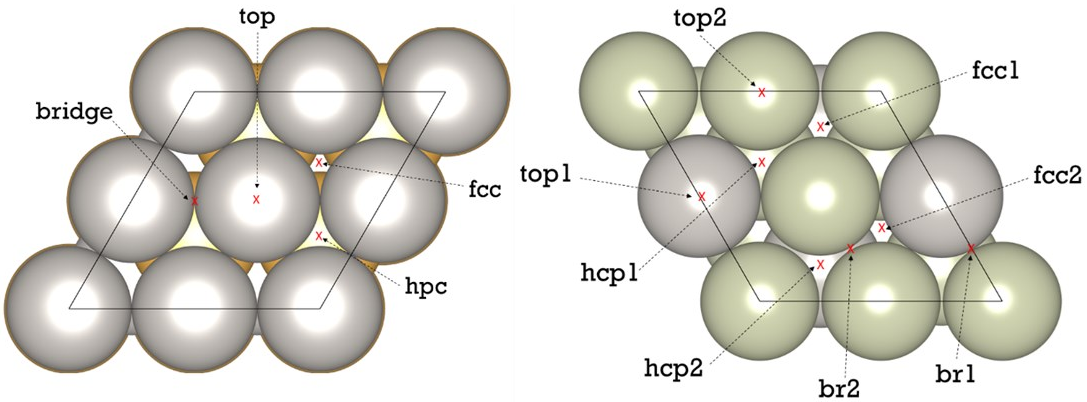

Figure 3. The symmetrical sites on the Pt (111) (left) and Rh_3Pt (111) (right) surfaces

Table 1. Adsorption energies (eV) of species on the Pt (111) surface.

Pt (111)	fcc	hcp	top	bridge	Preferential site
NO	-1.82	-1.61	-1.44	-1.82 (fcc)	fcc
N	-4.58	-4.31	-2.33	-4.59 (fcc)	fcc
O	-4.27	-3.87	-2.99	-4.28 (fcc)	fcc

The sites in brackets indicate the movement of species to these sites in the final states

comparison purpose. As seen from Table 2, two pseudopotentials give comparable adsorption energies. The most stable configuration for co-adsorption of N and O is N(fcc) and O(fcc) because the calculated adsorption energy for this configuration is the most thermodynamically favorable (-0.98 eV). It is also worth noting that some configurations of N and O lead to high reconstruction of the Pt (111) surface.

Next, the activation energy of the NO decomposition step: NO* ---> N* + O* on the Pt (111) surface was evaluated. The initial state is the NO located at the fcc site, and the final state is the co-adsorption of both N and O atoms at the fcc sites on the Pt (111) surface. They are shown in Figure 4. The activation energy for this step has been calculated via the nudged elastic band and climbing image – nudged elastic band methods implemented in Quantum ESPRESSO. Nine images have been interpolated between the initial and final images. The optimization scheme was selected to

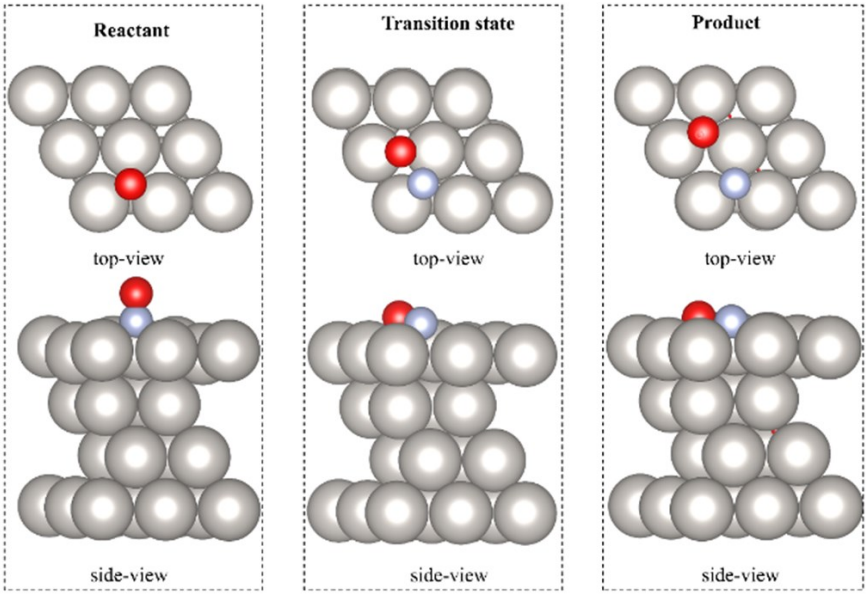

Figure 4. The initial (reactant), transition, and final (product) configurations of the NO decomposition on the Pt (111) surface. The blue, red, and violet spheres are nitrogen, oxygen, and platinum atoms, respectively.

Table 2. The adsorption energies of co-adsorption of N and O on the Pt (111) surface.

Initial configuration		Final configuration		BE, eV (kjpaw)	BE, eV (gbrv)
N	O	N	O		
fcc	fcc	fcc	fcc	-0.98	-1.01
fcc	hcp	fcc	br/hcp	-0.14	
fcc	top	fcc	top	-0.09	
fcc	br	fcc	fcc	-0.98	
hcp	fcc	br/hcp	fcc	-0.21	
hcp	hcp	hcp	hcp	-0.58	-0.61
hcp	br	hcp	hcp	-0.58	
hcp	top	hcp	top	0.16	
top	fcc	top	fcc	0.99	
top	top	fcc	fcc	-0.98	
top	br	hcp	fcc	-0.21	
top	hcp	top	hcp	1.37	1.32
br	fcc	fcc	fcc	-0.98	
br	br	fcc	fcc	-0.98	
br	hcp	hcp	hcp	-0.58	
br	top	fcc	top	-0.09	

BE = Binding energy (adsorption energy)

be quasi-Newton Broyden's second method. The stability of the initial state (reactant) and final state (product) has been verified through the phonon calculations at the Gamma point without any imaginary vibrations. The calculated phonon vibrations at the Gamma point of the Pt (111) slab, initial and final states are listed in Table S1 (Supporting Information). Their phonon vibrations at Gamma shows positive frequencies with three acoustic modes, confirming their stability at their ground states.

The activation energies calculated by NEB and CI-NEB are shown in Figure 5. The calculated forward and backward activation energies are 2.35 and 1.51 eV, respectively. The transition state for the NO decomposition reaction is shown in Figure 4. The transition state was confirmed through the phonon calculation at the Gamma point (Table S1) showing only one imaginary frequency at i450 cm^{-1}. The distance of N-O is 1.82 Å, and the shortest distances of Pt-N and Pt-O are 1.9 and 2.0 Å, respectively. It should be noted that the value of reaction barrier for NO dissociation on the Pt (111) surface depends on the NO surface coverage and the presence of other pre-adsorbed species. In our calculation, the surface coverage of NO is 0.25ML. The forward reaction barrier obtained from our calculation agrees with that from the previous report with the same NO coverage at 0.25 mL [9].

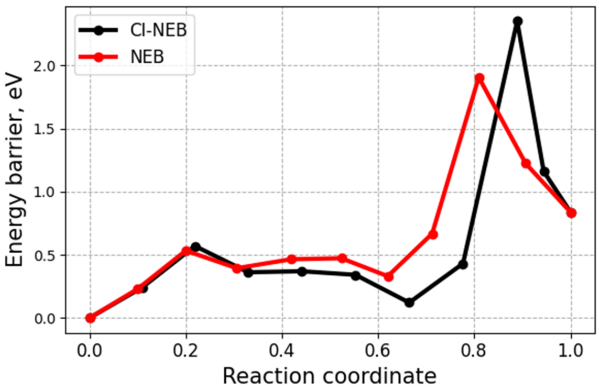

Figure 5. NEB and CI-NEB calculations for the reaction NO* ---> N* + O* on the Pt (111) surface

3.3 Preferential Adsorption Sites and Activation Energy on Rh_3Pt (111)

The adsorption energies of the NO molecule, N and O atoms on the Rh_3Pt (111) surface were calculated and are listed in Table 3. Three species prefer binding with the Rh_3Pt (111) surface at the fcc1 site. This hollow site is formed by three Rh atoms, as shown in Figure 3. The co-adsorption energies for the N and O atoms on the Rh_3Pt (111) surface were calculated and are presented in Table 4. It is worth noting that the binding energies of three species (NO, N, and O) on the Rh_3Pt (111) are stronger than those on the Pt (111).

The preferential adsorption sites for co-adsorption of N and O on Rh_3Pt (111) surface were examined in terms of adsorption energy. The calculated adsorption energies for co-adsorption of N and O on the symmetric sites of the Rh_3Pt (111) surface are listed in Table 4. The N and O atoms on different symmetrical sites are referred to as the initial configurations. After performing calculations, the positions of N and O were changed and moved to more energetically stable sites, and these sites are referred to as the final configurations. The preferential adsorption sites of co-adsorption of N and O on the Rh_3Pt (111) surface are N(hcp2)-O(fcc1) because the adsorption energy for this configuration is the most thermodynamically favorable (-2.83 eV). Knowing the initial and final states, the activation energy of the NO decomposition on the Rh_3Pt (111) surface was performed through the NEB and CI-NEB schemes. The initial and final states are shown in Figure 6.

The stability of the initial state (reactant) and final state (product) has been verified through the phonon calculations at the Gamma point without any imaginary vibrations. The calculated phonon vibrations at the Gamma point of the Rh_3Pt (111) slab, initial and final states are listed in Table S2 (Supporting Information). Their phonon vibrations at Gamma

Table 3. Adsorption energy (eV) of species on Rh_3Pt (111) surface

Rh_3Pt (111)	fcc1	fcc2	hcp1	hcp2	top1	top2	br1	br2	Preferential site
NO	-2.55	-2.50	-2.44	-2.50	-0.95	-1.97	-2.00	-2.44	fcc1
N	-5.61	-5.12	-5.18	-5.54	-2.64	-5.60 (fcc1)	-5.18 (hcp1)	-5.61 (fcc1)	fcc1
O	-5.33	-4.82	-4.64	-5.03	-3.04	-5.33 (fcc1)	-4.82 (fcc2)	-5.33 (fcc1)	fcc1

The sites in brackets indicate the movement of species to these sites in the final states

shows positive frequencies with three acoustic modes, confirming their stability at their ground states. The activation energies calculated by NEB and CI-NEB are shown in Figure 7. The calculated forward and backward activation energies are 2.02 and 2.30 eV, respectively. The transition state for the NO decomposition reaction is shown in Figure 6. The transition state was confirmed through the phonon calculation at the Gamma point (Table S2), showing only one imaginary frequency at i158 cm^{-1}. The distance of N-O is 2.15 Å, and the shortest distances of Rh-N and Rh-O are 1.66 and 1.96 Å, respectively.

The calculations suggest that the Rh_3Pt (111) surface not only provides a lower energy barrier for the NO decomposition but also gives a higher energy barrier for the recombination of N and O to form NO than the Pt (111) surface. In addition, the formation of N_2 or N_2O will be affected by the activation energy of the NO decomposition. For example, if the activation energy of the NO decomposition is higher than that of the N_2 or N_2O formation, as soon as NO starts dissociating to N and O, N_2 or N_2O will be produced. In contrast, high selectivity of N_2 or N_2O can be obtained by performing the NO decomposition reaction at elevated temperatures if the activation energy of N_2 or N_2O formation is higher than that of the NO decomposition reaction. The calculated activation energy of the NO decomposition on the Rh_3Pt (111) surface (2.02 eV) from our study is indeed lower than that of the NO decomposition on the Rh_3Ag (111) surface (~ 2.30 eV), $Rh_{15}Ag$ surface (~2.35 eV), or pure Rh (111) surface (2.69 eV) [17]. This observation contradicts the linear mixing rule because the resulting alloy enhances the reactivity for the NO decomposition on both Pt (111) and Rh (111) surfaces.

Table 4. The adsorption energies of co-adsorption of N and O on the Rh_3Pt (111) surface.

Initial		Final		BE, eV	Initial		Final		BE, eV
N	O	N	O		N	O	N	O	
fcc1	br1	fcc1	fcc2	-2.56	fcc2	br1	br2-NO*	br2-NO*	-1.84
fcc1	br2	top2-bottom	top2-top	-1.97	fcc2	br2	fcc2	fcc1	-2.56
fcc1	fcc2	fcc1	fcc2	-2.56	fcc2	fcc1	fcc2	fcc1	-2.56
fcc1	hcp1	fcc1	hcp1	-1.48	fcc2	hcp1	fcc2	fcc1	-2.56
fcc1	hcp2	fcc1	hcp2	-2.56	fcc2	hcp2	fcc2	hcp2	-1.47
fcc1	top1	fcc1	top1	-1.23	fcc2	top1	br1-bottom	br1-top	-2.31
fcc1	top2	fcc1-bottom	fcc1-top	-2.55	fcc2	top2	fcc2	NO*	-1.64
Initial		Final		BE, eV	Initial		Final		BE, eV
N	O	N	O		N	O	N	O	
hcp1	br1	hcp1	br1	-1.96	br1	br2	hcp1-NO*	hcp1-NO*	-1.69
hcp1	br2	fcc1	fcc1-top	-2.55	br1	fcc1	fcc2	fcc1	-2.56
hcp1	fcc2	hcp1	fcc2	-1.45	br1	fcc2	fcc2-N	fcc2	-1.65
hcp1	fcc1	hcp1	fcc1	-1.64	br1	hcp1	hcp1-NO*	hcp1-NO*	-1.69
hcp1	hcp2	hcp1	hcp2	-2.26	br1	hcp2	hcp2-NO*	hcp2-NO*	-2.26
hcp1	top1	br2	br2-top	-2.44	br1	top1	top2-NO*	top2-NO*	-1.97
hcp1	top2	hcp1	top2	-1.69	br1	top2	br1-NO*	br1-NO*	-1.39
Initial		Final		BE, eV	Initial		Final		BE, eV
N	O	N	O		N	O	N	O	
br2	br1	br2-NO*	br2-NO*	-2.44	hcp2	br1	hcp2	hcp1	-2.22
br2	fcc1	fcc1-NO*	fcc1-NO*	-2.55	hcp2	br2	hcp2	fcc1	-2.83
br2	fcc2	fcc1	fcc2	-2.56	hcp2	fcc2	hcp2	fcc2	-1.66
br2	hcp1	br2-NO*	br2-NO*	-2.44	hcp2	hcp1	hcp2	hcp1	-2.22
br2	hcp2	fcc1	hcp2	-2.56	hcp2	fcc1	hcp2	fcc1	-2.83
br2	top1	fcc1	top1	-1.23	hcp2	top1	hcp2	top1	-1.21
br2	top2	br2-NO*	br2-NO*	-1.89	hcp2	top2	hcp2	NO*	-1.96
Initial		Final		BE	Initial		Final		BE
N	O	N	O		N	O	N	O	
top1	br1	br1-NO*	b1-NO*	-1.39	top2	br1	top2	top2	-1.97
top1	br2	fcc2	fcc1	-2.56	top2	br2	br2-NO*	br2-NO*	-1.89
top1	fcc2	top1-NO*	top1-NO*	-1.34	top2	fcc2	top2	top2	-1.96
top1	hcp1	top1-NO*	top1-NO*	-1.34	top2	hcp1	br2-NO*	br2-NO*	-1.89
top1	fcc1	top1	fcc1	-0.46	top2	fcc1	top2-NO*	top2-NO*	-1.97
top1	hcp2	top1	hcp1	-0.20	top2	hcp2	top2-NO*	top2-NO*	-1.97
top1	top2	hcp2	fcc1	-2.83	top2	top1	fcc1	fcc2	-2.56
top1	br1	br1-NO*	b1-NO*	-1.39	top2	br1	top2	top2	-1.97

(*) indicates the formation of NO molecule; BE = binding energy (adsorption energy)

To understand the chemistry insights behind our observation for a lower activation energy of the NO decomposition reaction on the Rh_3Pt (111) surface than that on the Pt (111) surface, the projected density of states (PDOS) have been calculated for the Pt (5d) and Rh (4d) atoms from the top-most layer of the Pt (111) and Rh_3Pt (111) surfaces. The calculated results are shown in Figure 8. The molecular orbitals of NO are named as 4s, 1p, 5s, and 2π. For NO/Pt (111) and NO/Rh_3Pt (111), PDOS of Pt (5d) and Rh (4d) shows four new peaks corresponding to the hybridization of the molecular orbitals (4s, 1p, 5s, and 2π) of NO with *d*-band of the metals. In general, a stronger hybridization between *d*-band of the metal with three NO bonding orbitals (4s, 1p, 5s) results in stronger interaction between metallic surface and NO molecule. In contrast, a stronger hybridization between *d*-band of the metal with 2π* anti-bonding orbital of NO better weakens the N-O bond.

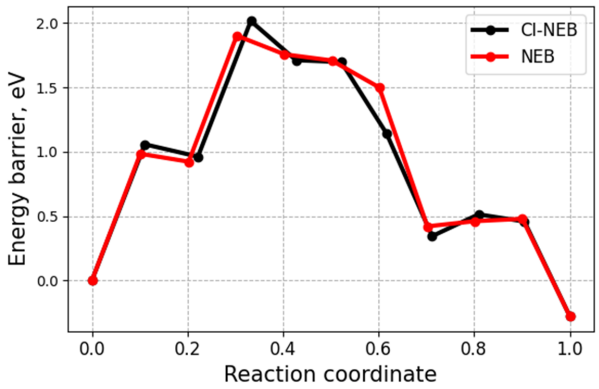

Figure 7. NEB and CI-NEB calculations for the reaction NO* ---> N* + O* on the Rh_3Pt (111) surface.

Figure 8 shows that the NO/Rh_3Pt (111) system has a stronger back-donation from electrons in *d*-orbital of Rh into the 2π* anti-bonding orbital of the adsorbed NO molecule than the NO/Pt (111) system. This facilitates the pre-cleavage of the N-O chemical bond on the Rh_3Pt (111) surface and leads to a lower activation energy of the NO decomposition. In addition, the weak signals of the molecular orbitals of NO from PDOS of Pt (5d) in the NO/Rh_3Pt (111) system indicate that NO mostly interacts with and is catalysed by the Rh active sites. This observation is consistent with the fact that the most stable adsorption position of NO on the Rh_3Pt (111) surface is fcc1.

4. Conclusion

Pt (111) and Rh_3Pt (111) catalytic surfaces have been investigated for the NO dissociation. The adsorption site of NO and co-adsorption sites of N and O on the Pt (111) surface locate

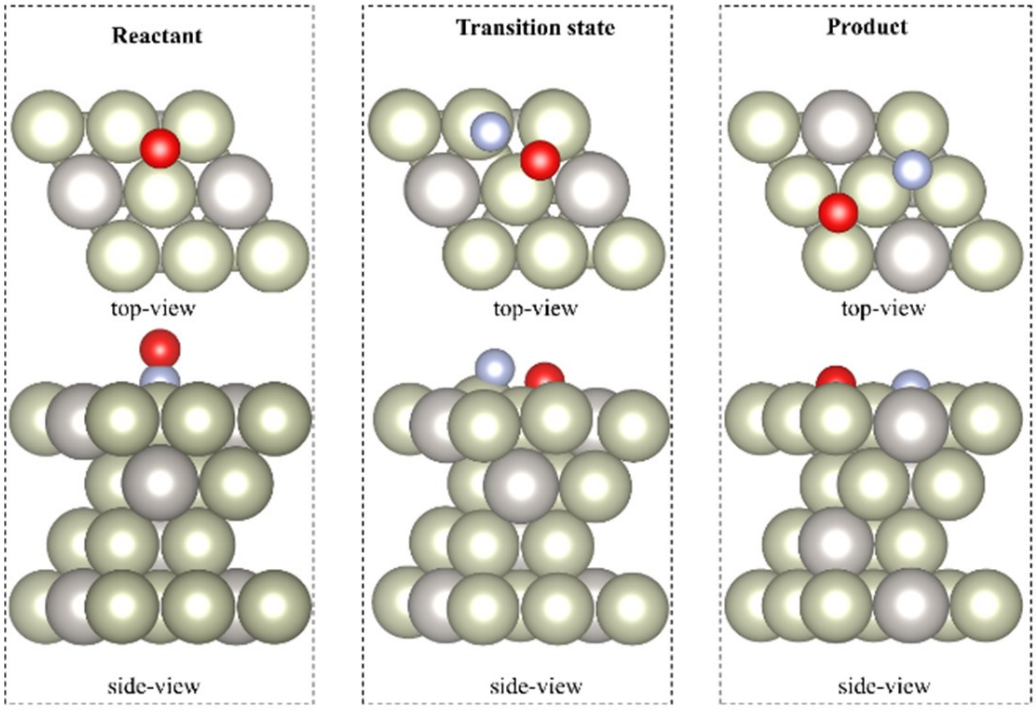

Figure 6. The initial (reactant), transition, and final (product) states of NO decomposition on the Rh3Pt (111) surface. The blue, red, gray, and violet spheres are nitrogen, oxygen, rhodium, and platinum atoms, respectively.

at the fcc sites. The preferential adsorption site of NO and co-adsorption sites of N and O on the Rh_3Pt (111) surface are: NO(fcc1) and N(hcp2)-O(fcc1). The activation energy of the NO dissociation on the Pt (111) and Rh_3Pt (111) surfaces are 2.35 and 2.03 eV, respectively. The transition states were confirmed by a single imaginary frequency in the phonon calculations. The calculated phonon vibrations for the bare and adsorbed surfaces of Pt (111) and Rh_3Pt (111) show that those surfaces are dynamically stable. This study shows that the addition of Rh metal into Pt metal to form an alloy provides an alternate route with a lower activation energy for the NO dissociation. The calculations of the projected density of states for Pt 5d and Rh 4d states revealed that the Rh_3Pt (111) surface has a lower activation energy for the NO decomposition than the Pt (111) surface because the 4d orbital in Rh has a stronger back-donation to the $2\pi^*$ anti-bonding orbital of the NO molecule.

Acknowledgment

This research is funded by Vietnam National University HoChiMinh City (VNU-HCM) under grant number C2022-28-09.

CRediT Author Statement

Khoa Thanh Phung: writing, reviewing and editing the manuscript; *Le Hoang Thong*: data analysis and editing the manuscript; *Bui Thi Linh*: data analysis and editing the manuscript; *Khanh B. Vu*: funding acquisition and management, performing calculations, writing the original manuscript, data processing; *Nguyen Ngoc Huyen*: data analysis and editing the manuscript. The manuscript has been read and agreed by all authors for submission.

References

[1] Han, L., Cai, S., Gao, M., Hasegawa, J.-y., Wang, P., Zhang, J., Shi, L., Zhang, D. (2019) Selective Catalytic Reduction of NOx with NH_3 by Using Novel Catalysts: State of the Art and Future Prospects. *Chemical Reviews*. 119 (19), 10916-10976. DOI: 10.1021/acs.chemrev.9b00202.

[2] Wang, Z., Kuang, H., Zhang, J., Chu, L., Ji, Y.. (2019) Nitrogen oxide removal by non-thermal plasma for marine diesel engines. *RSC Advances*. 9 (10), 5402-16. DOI: 10.1039/C8RA09217F.

[3] Rajanikanth, B.S., Mohapatro, S., Umanand, L. (2009) Solar powered high voltage energization for vehicular exhaust cleaning: A step towards possible retrofitting in vehicles. *Fuel Processing Technology*. 90 (3), 343-52. DOI: 10.1016/j.fuproc.2008.10.004.

[4] Suchak, N.J., Jethani, K., Joshi, J.B. (1990) Absorption of nitrogen oxides in alkaline solutions: selective manufacture of sodium nitrite. *Industrial & Engineering Chemistry Research*. 29 (7), 1492-502. DOI: 10.1021/ie00103a059.

[5] Yang, J.-R., Wang, Y., Chen, H., Ren, R.-P., Lv, Y.-K. (2021) A new approach for the effective removal of NOx from flue gas by using an integrated system of oxidation–absorption–biological reduction. *Journal of Hazardous Materials*. 404, 124109. DOI: 10.1016/j.jhazmat.2020.124109.

[6] Thomas, D., Vanderschuren, J. (2000) Nitrogen Oxides Scrubbing with Alkaline Solutions. *Chemical Engineering & Technology*. 23 (5), 449-455. DOI: 10.1002/(SICI)1521-4125(200005)23:5<449::AID-CEAT449>3.0.CO;2-L

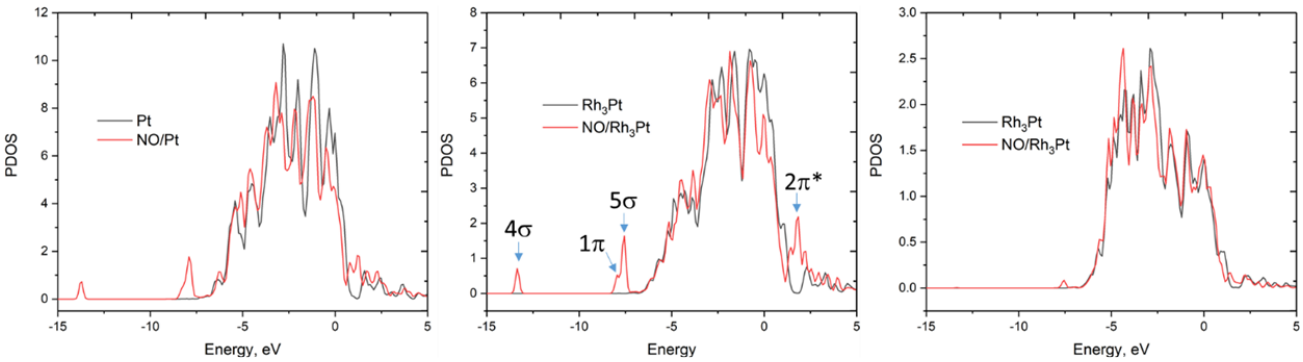

Figure 8. Projected density of states (PDOS) of the metallic atoms in the top-most layer of the Pt (111) and Rh_3Pt (111) surfaces. Left: Pt (5d) in Pt (111) and NO/Pt (111). Middle: Rh (4d) in Rh_3Pt (111) and NO/Rh_3Pt (111). Right: Pt (5d) in Rh_3Pt (111) and NO/Rh_3Pt (111). Fermi level was set to zero

[7] Yu, C., Yi, Y., Zhou, J., Xu, W. (2023) Highly effective and energy-saving removal of NO through an adsorption–microwave catalytic decomposition method under complex flue gas at low temperature. *Inorganic Chemistry Frontiers*. 10 (13), 3808-3820. DOI: 10.1039/D3QI00126A.

[8] Wang, X., Yang, X., Qiao, X., Guo, J., Guo, J., Jin, Y., Fan, B. (2020) Effect of Water Vapor on Catalytic Decomposition of NO over Cu–ZSM-5: A Mechanism and Kinetic Study. *Energy & Fuels*. 34 (9), 11341-11352. DOI: 10.1021/acs.energyfuels.0c01866.

[9] Cubides, D., Guimerà, X., Jubany, I., Gamisans, X. (2023) A review: Biological technologies for nitrogen monoxide abatement. *Chemosphere*. 311, 137147. DOI: 10.1016/j.chemosphere.2022.137147.

[10] Páez, D.F.C., Villalba, X.G., Zabalo, N.A., Galceran, H.T., Güell, I.J., Noguera, X.G. (2023) Mass transfer vectors for nitric oxide removal through biological treatments. *Environmental Science and Pollution Research*. 30 (51), 110089-1100103. DOI: 10.1007/s11356-023-30009-6.

[11] Lim, T., La, Y., Jeon, O.S., Park, S.Y., Yoo, Y.J., Yang, K.-H. (2020) Pore Structure Analysis to Adsorb NOx Gas based on Porous Materials. *Journal of the Korean Physical Society*. 77 (9), 790-796. DOI: 10.3938/jkps.77.790.

[12] Wakabayashi, R., Tomita, A., Kimura, T. (2020) Understanding of NOx storage property of impregnated Ba species after crystallization of mesoporous alumina powders. *Journal of Hazardous Materials*. 398, 122791. DOI: 10.1016/j.jhazmat.2020.122791.

[13] Xiao, B., Wheatley, P.S., Zhao, X., Fletcher, A.J., Fox, S., Rossi, A.G., Megson, I.L., Bordiga, S., Regli, L., Thomas, K.M., Morris, R.E. (2007) High-Capacity Hydrogen and Nitric Oxide Adsorption and Storage in a Metal−Organic Framework. *Journal of the American Chemical Society*. 129 (5), 1203-1209. DOI: 10.1021/ja066098k.

[14] Amirnazmi, A., Boudart, M. (1975). Decomposition of nitric oxide on platinum. *Journal of Catalysis*. 39 (3), 383-394. DOI: 10.1016/0021-9517(75)90305-X.

[15] Granger, P., Wu, J., Ba, H., Baaziz, W., Ersen, O., Zafeiratos, S., Nhut, J.-M., Giambastiani, G., Pham-Huu, C. (2021) Cooperative effect of Pt single-atoms and nanoparticles supported on carbonaceous materials: Catalytic NO decomposition as a probe reaction. *Applied Catalysis A: General*. 617, 118103. DOI: 10.1016/j.apcata.2021.118103.

[16] Bakker, J.M., Mafuné, F. (2022) Zooming in on the initial steps of catalytic NO reduction using metal clusters. *Physical Chemistry Chemical Physics*. 24 (13), 7595-7610. DOI: 10.1039/D1CP05760J.

[17] Inderwildi, O.R., Jenkins, S.J., King, D.A. (2007) When adding an unreactive metal enhances catalytic activity: NOx decomposition over silver–rhodium bimetallic surfaces. *Surface Science*. 601 (17), L103-L108. DOI: 10.1016/j.susc.2007.06.031.

[18] Reddy, G.K., Ling, C., Peck, T.C., Jia, H. (2017) Understanding the chemical state of palladium during the direct NO decomposition – influence of pretreatment environment and reaction temperature. *RSC Advances*. 7 (32), 19645-19655. DOI: 10.1039/C7RA00836H.

[19] Toso, A., Danielis, M., de Leitenburg, C., Boaro, M., Trovarelli, A., Colussi, S. (2022) Key Properties and Parameters of Pd/CeO_2 Passive NO_x Adsorbers. *Industrial & Engineering Chemistry Research*. 61 (9), 3329-3341. DOI: 10.1021/acs.iecr.1c04805.

[20] Fang, S., Takagaki, A., Watanabe, M., Ishihara, T. (2020) The direct decomposition of NO into N_2 and O_2 over copper doped $Ba_3Y_4O_9$. *Catalysis Science & Technology*. 10 (8), 2513-2522. DOI: 10.1039/D0CY00194E.

[21] Liu, Y., Chen, L., Liu, S., Yang, S., Shangguan, J. (2023) Role of iron-based catalysts in reducing NO_x emissions from coal combustion. *Chinese Journal of Chemical Engineering*. 59, 1-8. DOI: 10.1016/j.cjche.2022.11.017.

[22] Williamson, W.B., Stepien, H.K., Gandhi, H.S. (1980) Poisoning of platinum-rhodium automotive three-way catalysts: behavior of single-component catalysts and effects of sulfur and phosphorus. *Environmental Science & Technology*. 14 (3), 319-324. DOI: 10.1021/es60163a008.

[23] Matsumoto, Y., Onishi, T., Tamaru, K. (1980) Effects of sulphur on a palladium surface on the adsorption of carbon monoxide and the adsorption and decomposition of nitric oxide. *Journal of the Chemical Society, Faraday Transactions 1: Physical Chemistry in Condensed Phases*. 76 (0), 1116-1121. DOI: 10.1039/F19807601116.

[24] Spassova, I., Khristova, M., Nyagolova, N., Mehandjiev, D. (2000) Decomposition of NO over copper-manganese oxide catalysts at room temperature. In: Corma A, Melo FV, Mendioroz S, Fierro JLG (editors). *Studies in Surface Science and Catalysis*. 130: Elsevier; 2000. p. 1313-8. DOI: 10.1016/S0167-2991(00)80381-X

[25] Zhao, P., Ehara, M. (2023) Theoretical insights into the support effect on the NO activation over platinum-group metal catalysts. *The Journal of Chemical Physics*. 158 (13). DOI: 10.1063/5.0145586.

[26] Burch, R., Breen, J.P., Meunier, F.C. (2002) A review of the selective reduction of NO_x with hydrocarbons under lean-burn conditions with non-zeolitic oxide and platinum group metal catalysts. *Applied Catalysis B: Environmental*. 39 (4), 283-303. DOI: 10.1016/S0926-3373(02)00118-2.

[27] Castoldi, L., Matarrese, R., Kubiak, L., Daturi, M., Artioli, N., Pompa, S., Lietti, L. (2019) In-depth insights into N_2O formation over Rh- and Pt-based LNT catalysts. *Catalysis Today*. 320, 141-151. DOI: 10.1016/j.cattod.2018.01.026.

[28] Cho, B.K. (1994) Mechanistic Importance of Intermediate N_2O + CO Reaction in Overall NO + CO Reaction System: II. Further Analysis and Experimental Observations. *Journal of Catalysis*. 148 (2), 697-708. DOI: 10.1006/jcat.1994.1256.

[29] Cho, B.K. (1992) Mechanistic importance of intermediate N_2O + CO reaction in overall NO + CO reaction system: I. Kinetic analysis. *Journal of Catalysis*. 138 (1),255-266. DOI: 10.1016/0021-9517(92)90021-9.

[30] Liu, Z.-P., Jenkins, S.J., King, D.A. (2003) Step-Enhanced Selectivity of NO Reduction on Platinum-Group Metals. *Journal of the American Chemical Society*. 125 (48), 14660-14661. DOI: 10.1021/ja0372208.

[31] Bai, Y., Mavrikakis. M. (2018) Mechanistic Study of Nitric Oxide Reduction by Hydrogen on Pt(100) (I): A DFT Analysis of the Reaction Network. *The Journal of Physical Chemistry B*. 122 (2), 432-443. DOI: 10.1021/acs.jpcb.7b01115.

[32] Gonzalez, J.D., Shojaee, K., Haynes, B.S., Montoya, A. (2018) The effect of surface coverage on N_2, NO and N_2O formation over Pt(111). *Physical Chemistry Chemical Physics*. 20 (39), 25314-25323. DOI: 10.1039/C8CP04066D.

[33] Farberow, C.A., Dumesic, J.A., Mavrikakism, M. (2014) Density Functional Theory Calculations and Analysis of Reaction Pathways for Reduction of Nitric Oxide by Hydrogen on Pt(111). *ACS Catalysis*. 4 (10), 3307-3319. DOI: 10.1021/cs500668k.

[34] Ungerer, M.J., Santos-Carballal, D., Cadi-Essadek, A., van Sittert, C.G.C.E., de Leeuw, N.H. (2019) Interaction of H_2O with the Platinum Pt (001), (011), and (111) Surfaces: A Density Functional Theory Study with Long-Range Dispersion Corrections. *The Journal of Physical Chemistry C.* 123 (45), 27465-27476. DOI: 10.1021/acs.jpcc.9b06136.

[35] Chen, J.-J., Wang, S.-D., Li, Z.-Y., Li, X.-N., He, S.-G. (2023) Selective Reduction of NO into N_2 Catalyzed by Rh1-Doped Cluster Anions $RhCe_2O_{3-5}^-$. *Journal of the American Chemical Society*. 2023. DOI: 10.1021/jacs.3c06565.

[36] Tiri, R.N.E., Aygün, A., Gülbay, S.K., Sen, F., Cheng, C.K., Jafarzadeh, H., Abouei Mehrizi, A., Vasseghian, Y. (2022) Improving hydrogen generation from dehydrogenation of dimethylamine borane using polyvinylpyrrolidone stabilized platinum-rhodium nanoclusters as highly efficient and reusable catalysts: Development of ANN model. *Chemical Engineering Research and Design*. 182, 305-311. DOI: 10.1016/j.cherd.2022.04.005.

[37] Yan, Q., Wang, X.-Y., Feng, J.-J., Mei, L.-P., Wang, A.-J. (2021) Simple fabrication of bimetallic platinum-rhodium alloyed nanomultipods: A highly effective and recyclable catalyst for reduction of 4-nitrophenol and rhodamine B. *Journal of Colloid and Interface Science*. 582, 701-710. DOI: 10.1016/j.jcis.2020.08.062.

[38] Devendra, B.K., Praveen, B.M., Tripathi, V.S., Nagaraju, G., Nagaraju, D.H., Nayana, K.O. (2021) Highly corrosion resistant platinum-rhodium alloy coating and its photocatalytic activity. *Inorganic Chemistry Communications*. 134, 109065. DOI: 10.1016/j.inoche.2021.109065.

[39] Han, Z., Zhang, R.-L., Duan, J.-J., Wang, A.-J., Zhang, Q.-L., Huang, H., Feng, J.-J. (2019) Platinum-rhodium alloyed dendritic nanoassemblies: An all-pH efficient and stable electrocatalyst for hydrogen evolution reaction. *International Journal of Hydrogen Energy*. 45 (11), 6110-6119. DOI: 10.1016/j.ijhydene.2019.12.155.

[40] Giannozzi, P., Baroni, S., Bonini, N., Calandra, M., Car, R., Cavazzoni, C., Ceresoli, D., Chiarotti, G. L., Cococcioni, M., Dabo, I., Dal Corso, A., de Gironcoli, S., Fabris, S., Fratesi, G., Gebauer, R., Gerstmann, U., Gougoussis, C., Kokalj, A., Lazzeri, M., Martin-Samos, L., Marzari, N., Mauri, F., Mazzarello, R., Paolini, S., Pasquarello, A., Paulatto, L., Sbraccia, C., Scandolo, S., Sclauzero, G., Seitsonen, A. P., Smogunov, A., Umari, P., Wentzcovitch, R. M. (2009) QUANTUM ESPRESSO: a modular and open-source software project for quantum simulations of materials. *Journal of Physics: Condensed Matter*. 21 (39), 395502. DOI: 10.1088/0953-8984/21/39/395502.

[41] Giannozzi, P., Andreussi, O., Brumme, T., Bunau, O., Buongiorno Nardelli, M., Calandra, M., Car, R., Cavazzoni, C., Ceresoli, D., Cococcioni, M., Colonna, N., Carnimeo, I., Dal Corso, A., de Gironcoli, S., Delugas, P., DiStasio, R.A., Ferretti, A., Floris, A., Fratesi, G., Fugallo, G., Gebauer, R., Gerstmann, U., Giustino, F., Gorni, T., Jia, J., Kawamura, M., Ko, H.Y., Kokalj, A., Küçükbenli, E., Lazzeri, M., Marsili, M., Marzari, N., Mauri, F., Nguyen, N.L., Nguyen, H.V., Otero-de-la-Roza, A., Paulatto, L., Poncé, S., Rocca, D., Sabatini, R., Santra, B., Schlipf, M., Seitsonen, A.P., Smogunov, A., Timrov, I., Thonhauser, T., Umari, P., Vast, N., Wu, X., Baroni, S. (2017) Advanced capabilities for materials modelling with Quantum ESPRESSO. *Journal of Physics: Condensed Matter*. 29 (46), 465901. DOI: 10.1088/1361-648X/aa8f79.

[42] Kresse, G., Joubert, D. (1999) From ultrasoft pseudopotentials to the projector augmented-wave method. *Physical Review B*. 59 (3), 1758-1775. DOI: 10.1103/PhysRevB.59.1758.

[43] Vanderbilt, D. (1990) Soft self-consistent pseudopotentials in a generalized eigenvalue formalism. *Physical Review B*. 41 (11), 7892-7895. DOI: 10.1103/PhysRevB.41.7892.

[44] Ford, D.C., Xu, Y., Mavrikakis, M. (2005) Atomic and molecular adsorption on Pt(111). *Surface Science*. 587 (3), 159-174. DOI: 10.1016/j.susc.2005.04.028.